INTERNATIONAL JOURNAL OF ROBUST AND NONLINEAR CONTROL
Int. J. Robust Nonlinear Control 2010; **20**:489–503
Published online 16 April 2009 in Wiley InterScience (www.interscience.wiley.com). DOI: 10.1002/rnc.1438

Quaternion-based visual servo control in the presence of camera calibration error

Guoqiang Hu[1,*,†], Nicholas Gans[2] and Warren Dixon[2]

[1]*Department of Mechanical and Nuclear Engineering, Kansas State University, Manhattan, KS 66506, U.S.A.*
[2]*Department of Mechanical and Aerospace Engineering, University of Florida, Gainesville, FL 32611-6250, U.S.A.*

SUMMARY

Visual servo control systems use information from images along with knowledge of the optic parameters (i.e. camera calibration) to position the camera relative to some viewed object. If there are inaccuracies in the camera calibration, then performance degradation and potentially unpredictable response from the visual servo control system may occur. Motivated by the desire to incorporate robustness to the camera calibration, different control methods have been developed. Previous adaptive/robust controllers (especially for six degree-of-freedom camera motion) rely heavily on properties of the rotation parameterization to formulate state estimates and a measurable closed-loop error system. All of these results are based on the singular axis–angle parameterization. Motivated by the desire to express the rotation by a non-singular parameterization, efforts in this paper address the question: *Can state estimates and a measurable closed-loop error system be crafted in terms of the quaternion parameterization when the camera calibration parameters are unknown*? To answer this question, a contribution of this paper is the development of a robust controller and closed-loop error system based on a new quaternion-based estimate of the rotation error. A Lyapunov-based analysis is provided which indicates that the controller yields asymptotic regulation of the rotation and translation error signals given a sufficient approximate of the camera calibration parameters. Simulation results are provided that illustrate the performance of the controller for a range of calibration uncertainty. Copyright © 2009 John Wiley & Sons, Ltd.

Received 9 July 2007; Revised 15 July 2008; Accepted 18 December 2008

KEY WORDS: robust control; visual servo control; nonlinear system; Lyapunov methods; uncertain systems

1. INTRODUCTION

When a camera takes a picture, the appearance of the objects in the image depends on the position and orientation (i.e. pose) and optic parameters of the camera. Based on this fact, visual servo control systems use information from images along with knowledge of the optic parameters (i.e. camera calibration) to regulate the camera to a desired pose. One important issue that has limited the robustness of vision-based control systems is the potential for corrupt sensor data due to the lack of exact camera calibration. Exact calibration is often assumed so that the image-space

*Correspondence to: Guoqiang Hu, Department of Mechanical and Nuclear Engineering, Kansas State University, Manhattan, KS 66506, U.S.A.
†E-mail: gqhu@ksu.edu

Contract/grant sponsor: The NSF CAREER; contract/grant number: CMS-0547448
Contract/grant sponsor: AFOSR; contract/grant numbers: F49620-03-1-0381, F49620-03-1-0170
Contract/grant sponsor: AFRL; contract/grant number: FA4819-05-D-0011
Contract/grant sponsor: BARD; contract/grant number: US-3715-05
Contract/grant sponsor: The United States–Israel Binational Agricultural Research and Development Fund
Contract/grant sponsor: The Startup Fund

sensor measurements can be related to the Euclidean or joint-space for control computations. To relate the image-space to the Euclidean-space, both intrinsic and extrinsic parameters[‡] of the optic model are required. If these parameters are not exactly known, then performance degradation and potentially unpredictable response from the system may occur.

Motivated by the desire to incorporate robustness to the camera calibration, different control approaches have been proposed. For example, the results in [1–8] compensate for uncertainty in the camera calibration parameters, but they are constrained to planar visual servo control applications. Other approaches have been developed for six degree-of-freedom (DOF) camera motion through strategic manipulation and estimation of the image-Jacobian (i.e. interaction matrix). For example, new adaptive controllers for image-Jacobian-based control of a robot manipulator are developed in [9–11]. One problem with methods based on the image-Jacobian is that the estimated image-Jacobian may contain singularities. The development in [9] exploits an additional potential force function to drive the estimated parameters away from the values that result in a singular Jacobian matrix. Piepmeier *et al.* published a series of papers (e.g. see [12–16]) that exploit dynamic quasi-Newton recursive least-squares estimators to solve a variety of visual servo control problems despite an uncertain kinematic model and uncertainty in the camera model. In [17], Shahamiri and Jagersand used a nullspace-biased Newton-step visual servo strategy with a Broyden-type Jacobian estimation for online singularity detection and avoidance in an uncalibrated visual servo control problem. Through an innovative projection to a camera calibration invariant space, the results in [18] illustrate how a task function approach can be used to develop a local asymptotic visual servo controller under the assumption of a full rank image Jacobian (i.e. interaction matrix) and full rank estimated image Jacobian. The results in [18] are based on the additional assumption that the vector of invariant feature points is sufficiently close to the associated vector generated from a goal image so that a linear time-varying system can be analyzed.

One method to avoid potential singularities in the image Jacobian is to develop an error system that is composed of both reconstructed Euclidean information and image-space information, as in the seminal work in [19]. Motivated by the work in [19], the results in [20] and [21] illustrate how sufficiently good static estimates of the intrinsic calibration parameters could be used to develop homography-based visual servoing methods that achieve exponential or asymptotic regulation with respect to both camera and hand–eye calibration errors for the six DOF problem. Specifically, the authors of [21] relied on linearization methods (e.g. [21, Theorem 2]) or perturbation-based analysis methods to conclude local asymptotic stability. In [20], the class of controllers in [21] was extended to include controllers that yield exponential translation based on a nonlinear Lyapunov-based approach. Both of the results in [20, 21] rely heavily on properties of the axis–angle rotation parameterization to formulate state estimates and a measurable closed-loop error system in the presence of uncertainty in the camera calibration.

Motivated by applications where a non-singular rotation parameterization is desired/required (e.g. satellite attitude control), we recently introduced a new quaternion-based visual servo controller for the rotation error system in [22], under the assumption that the camera calibration parameters are exactly known. The results in this paper are motivated by the question: *Can state estimates and a measurable closed-loop error system be crafted in terms of the quaternion parameterization when the camera calibration parameters are unknown*? To answer this question, a contribution of this paper is the development of a quaternion-based estimate for the rotation error system that is related to the actual rotation error, the development of a new closed-loop error system, and a new Lyapunov-based analysis that demonstrates the stability of the quaternion error system. One of the challenges is to develop a quaternion estimate from an estimated rotation matrix that is generally not a true rotation matrix. To address this challenge, the similarity relationship between the estimated and actual rotation matrices is used (as in [20, 21]) to construct the relationship between the estimated and

[‡]The camera calibration parameters are composed of the so-called intrinsic parameters (i.e. image center, camera scale factors, and camera magnification factor) and extrinsic parameters (i.e. camera position and orientation).

DOI: 10.1002/rnc

actual quaternions. A Lyapunov-based stability analysis is provided which indicates that a unique controller can be developed to achieve the regulation result despite a sign ambiguity in the developed quaternion estimate. The stability analysis is predicated on the same condition given in [20, 21] that the static estimate of the calibration matrix is sufficiently close to the actual values. Simulation results illustrate the performance of the developed controller in the presence of reasonable calibration errors. The closed-loop errors are also shown to converge in additional simulations where the calibration parameters are an order of magnitude too small or too large. Order of magnitude calibration errors are well beyond typical inaccuracies, and these results give an indication of the mildness of sufficient condition on the static calibration estimate.

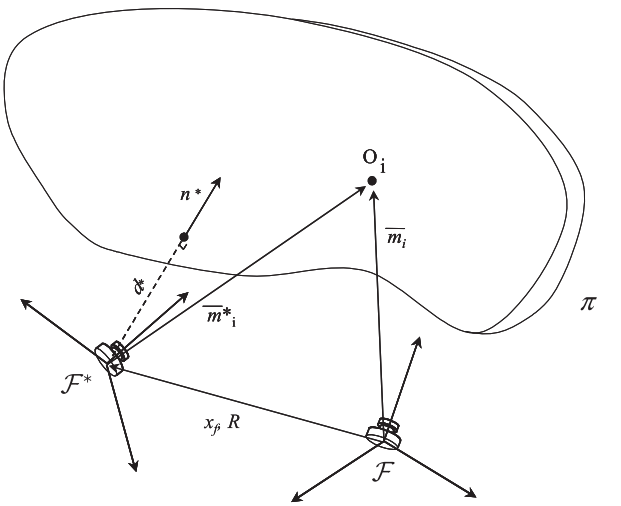

Figure 1. Coordinate frame relationships between a camera viewing a planar patch at different spatiotemporal instances.

2. EUCLIDEAN AND IMAGE-SPACE RELATIONSHIPS

Without loss of generality,[§] the subsequent development is based on the assumption that four stationary coplanar and non-collinear feature points [24] denoted by O_i $\forall i = 1, 2, 3, 4$ can be determined from a feature point tracking algorithm (e.g. Kanade–Lucas–Tomasi (KLT) algorithm discussed in [25, 26]). The plane defined by the four feature points is denoted by π as depicted in Figure 1. A coordinate frame $\mathcal{F}$ is considered to be affixed to the single current camera viewing the object, and a stationary coordinate frame $\mathcal{F}^*$ denotes a constant (*a priori* determined) desired camera position and orientation that is defined by a desired image. The Euclidean coordinates of the feature points O_i expressed in the frames $\mathcal{F}$ and $\mathcal{F}^*$ are denoted by $x_i(t), y_i(t), z_i(t) \in \mathbb{R}$ and $x_i^*, y_i^*, z_i^* \in \mathbb{R}$, respectively. The normalized Euclidean coordinate vectors, denoted by $m_i(t) \in \mathbb{R}^3$ and $m_i^* \in \mathbb{R}^3$, are defined as

$$m_i \triangleq \left[\frac{x_i}{z_i} \quad \frac{y_i}{z_i} \quad 1 \right]^{\mathrm{T}} \tag{1}$$

$$m_i^* \triangleq \left[\frac{x_i^*}{z_i^*} \quad \frac{y_i^*}{z_i^*} \quad 1 \right]^{\mathrm{T}} \tag{2}$$

with the standard assumption that the norm of m_i^* is bounded, $z_i(t) > \delta_1$ and $\delta_1 < z_i^* < \delta_2$, where δ_1, δ_2 are two positive constants. From standard Euclidean geometry, relationships between $m_i(t)$ and m_i^* can be determined as [24]

$$m_i = \underbrace{\frac{z_i^*}{z_i}}_{\alpha_i} \underbrace{(R + x_h n^{*\mathrm{T}})}_{H} m_i^* \tag{3}$$

where $\alpha_i(t) \in \mathbb{R}$ is a scaling term and $H(t) \in \mathbb{R}^{3\times 3}$ denotes the Euclidean homography. The Euclidean homography is composed of a scaled translation vector $x_h(t) \in \mathbb{R}^3$ expressed in $\mathcal{F}$, the rotation between $\mathcal{F}$ and $\mathcal{F}^*$ denoted by $R(t) \in SO(3)$, and $n^* \in \mathbb{R}^3$ denotes a constant unit normal to the plane π.

Each feature point O_i on π also has a pixel coordinate $p_i(t) \in \mathbb{R}^3$ and $p_i^* \in \mathbb{R}^3$ expressed in the image

[§] Image processing techniques can be used to select coplanar and non-collinear feature points within an image. However, if four coplanar target points are not available then the subsequent development can also exploit the virtual parallax algorithm [23] with no four of the eight target points being coplanar.

DOI: 10.1002/rnc

coordinate frame for the current image and the desired image denoted by

$$p_i \triangleq [u_i \;\; v_i \;\; 1]^{\mathrm{T}} \tag{4}$$

$$p_i^* \triangleq [u_i^* \;\; v_i^* \;\; 1]^{\mathrm{T}} \tag{5}$$

where $u_i(t), v_i(t), u_i^*, v_i^* \in \mathbb{R}$. The pixel coordinates $p_i(t)$ and p_i^* are related to the normalized task-space coordinates $m_i(t)$ and m_i^* by the following global invertible transformation (i.e. the pinhole camera model):

$$p_i = Am_i, \quad p_i^* = Am_i^* \tag{6}$$

where $A \in \mathbb{R}^{3\times 3}$ is a constant, upper triangular, and invertible intrinsic camera calibration matrix that is explicitly defined as [27]

$$A \triangleq \begin{bmatrix} \alpha & -\alpha\cot\phi & u_0 \\ 0 & \dfrac{\beta}{\sin\phi} & v_0 \\ 0 & 0 & 1 \end{bmatrix} \tag{7}$$

In (7), $u_0, v_0 \in \mathbb{R}$ denote the pixel coordinates of the principal point (i.e. the image center that is defined as the frame buffer coordinates of the intersection of the optical axis with the image plane), $\alpha, \beta \in \mathbb{R}$ represent the product of the camera scaling factors and the focal length, and $\phi \in \mathbb{R}$ is the skew angle between the camera axes.

3. FEEDBACK CONTROL MEASUREMENTS

The objective in this paper is to develop a kinematic controller (i.e. the control inputs are considered the linear and angular camera velocities) to ensure that the position/orientation of the camera coordinate frame $\mathcal{F}$ is regulated to the desired position/orientation $\mathcal{F}^*$. The only required sensor measurements for the control development are the image coordinates of the determined feature points (i.e. measurement of the signals in (4)), where the static feature point coordinates in the desired image are given *a priori*. By measuring the current image feature points and given the desired feature points, the relationship in (6) can be used to determine the normalized Euclidean coordinates of O_i provided that the intrinsic camera calibration matrix is perfectly known. Unfortunately, any uncertainty in A will lead to a corrupted measurement of $m_i(t)$ and m_i^*. The computed normalized coordinates are actually estimates, denoted by $\hat{m}_i(t), \hat{m}_i^* \in \mathbb{R}^3$, of the true values since only an invertible best-guess estimate of A, denoted by $\hat{A} \in \mathbb{R}^{3\times 3}$, is available in practice. The normalized coordinate estimates can be expressed as [21]

$$\hat{m}_i = \hat{A}^{-1} p_i = \tilde{A} m_i \tag{8}$$

$$\hat{m}_i^* = \hat{A}^{-1} p_i^* = \tilde{A} m_i^* \tag{9}$$

where the calibration error matrix $\tilde{A} \in \mathbb{R}^{3\times 3}$ is defined as

$$\tilde{A} = \hat{A}^{-1} A = \begin{bmatrix} \tilde{A}_{11} & \tilde{A}_{12} & \tilde{A}_{13} \\ 0 & \tilde{A}_{22} & \tilde{A}_{23} \\ 0 & 0 & 1 \end{bmatrix} \tag{10}$$

where $\tilde{A}_{11}, \tilde{A}_{12}, \tilde{A}_{13}, \tilde{A}_{22}, \tilde{A}_{23} \in \mathbb{R}$ denote unknown intrinsic calibration mismatch constants. As $m_i(t)$ and m_i^* cannot be exactly determined, the estimates in (8) and (9) can be substituted into (3) to obtain the following relationship:

$$\hat{m}_i = \alpha_i \hat{H} \hat{m}_i^* \tag{11}$$

where $\hat{H}(t) \in \mathbb{R}^{3\times 3}$ denotes the estimated Euclidean homography [21] defined as

$$\hat{H} = \tilde{A} H \tilde{A}^{-1} \tag{12}$$

As $\hat{m}_i(t)$ and $\hat{m}_i^*$ can be determined from (8) and (9), a set of 12 linear equations can be developed from the four image point pairs, and (11) can be used to solve for $\hat{H}(t)$ (see [28] for additional details regarding the set of linear equations). Provided that additional information is available (e.g. at least four vanishing points), various techniques (e.g. see [29, 30]) can be used to decompose $\hat{H}(t)$ to obtain the estimated rotation and translation components as follows:

$$\begin{aligned} \hat{H} &= \tilde{A} R \tilde{A}^{-1} + \tilde{A} x_h n^{*T} \tilde{A}^{-1} \\ &= \hat{R} + \hat{x}_h \hat{n}^{*T} \end{aligned} \tag{13}$$

DOI: 10.1002/rnc

where $\hat{R}(t) \in \mathbb{R}^{3\times 3}$ is defined as [20, 21]

$$\hat{R} = \tilde{A} R \tilde{A}^{-1} \tag{14}$$

and $\hat{x}_h(t) \in \mathbb{R}^3, \hat{n}^* \in \mathbb{R}^3$ denote the estimate of $x_h(t)$ and n^*, respectively, defined as

$$\hat{x}_h = \sigma \tilde{A} x_h \tag{15}$$

$$\hat{n}^* = \frac{1}{\sigma} \tilde{A}^{-\mathrm{T}} n^* \tag{16}$$

where $\sigma \in \mathbb{R}$ denotes the following positive constant:

$$\sigma = \| \tilde{A}^{-\mathrm{T}} n^* \| \tag{17}$$

4. CONTROL OBJECTIVE

As stated previously, the objective in this paper is to develop a kinematic controller to ensure that the position/orientation of the camera coordinate frame $\mathcal{F}$ is regulated to the desired position/orientation $\mathcal{F}^*$ despite uncertainty in the intrinsic camera calibration matrix. This objective is based on the assumption that the linear and angular velocities of the camera are control inputs that can be independently controlled (i.e. unconstrained motion). For example, the linear and angular camera velocities could be controlled by the end-effector of a robotic manipulator. In addition to uncertainty in the intrinsic camera calibration, uncertainty could also exist in the extrinsic camera calibration (e.g. the uncertainty in the rotation and translation of the camera with respect to the robot end-effector). The development in this paper could be directly modified as described in [20, 21] to compensate for the extrinsic calibration. Therefore, the effects of a mismatch in the extrinsic calibration are not considered in the subsequent development for simplicity.

In the Euclidean space, the rotation control objective can be quantified as

$$R(t) \to I_3 \quad \text{as } t \to \infty \tag{18}$$

The subsequent development is formulated in terms of the four-dimensional unit quaternion defined as

$$q \triangleq [q_0 \;\; q_v^{\mathrm{T}}]^{\mathrm{T}} \tag{19}$$

In (19), $q_v(t) \triangleq [q_{v1}(t) \;\; q_{v2}(t) \;\; q_{v3}(t)]^{\mathrm{T}}, q_0(t), q_{vi}(t) \in \mathbb{R}$ $\forall i = 1, 2, 3$, where the unit quaternion must also satisfy the following nonlinear constraint:

$$q^{\mathrm{T}} q = 1 \tag{20}$$

Given the rotation matrix $R(t)$, the corresponding unit quaternion $q(t)$ can be calculated by using the numerically robust method presented in [22, 31] based on the corresponding relationship

$$\begin{aligned} R(q) &= I_3 - 2q_0 q_v^{\times} + 2(q_v^{\times})^2 \\ &= (q_0^2 - q_v^{\mathrm{T}} q_v) I_3 + 2 q_v q_v^{\mathrm{T}} - 2 q_0 q_v^{\times} \end{aligned} \tag{21}$$

where I_3 is the 3×3 identity matrix, and the notation $q_v^{\times}(t)$ denotes the following skew-symmetric form of the vector $q_v(t)$ [22].

From (20) and (21), the rotation regulation objective in (18) can also be quantified as the desire to regulate $q_v(t)$ as

$$\| q_v(t) \| \to 0 \quad \text{as } t \to \infty \tag{22}$$

The focus and contribution of this paper lie in the ability to develop and prove the stability of a quaternion-based rotation controller in the presence of uncertainty in the camera calibration. The translation controller developed in [20] is also presented and incorporated in the stability analysis to provide an example of how the new class of quaternion-based rotation controllers can be used in conjunction with translation controllers that are robust to camera calibration uncertainty including (for example): the asymptotic translation controllers in [21] and the exponential translation controllers in [20]. The translation error, denoted by $e(t) \in \mathbb{R}^3$, is defined as [20, 21]

$$e = \frac{z_i}{z_i^*} m_i - m_i^* \tag{23}$$

where i denotes any of the four feature points (i.e. the error vector only needs to be defined for a single feature point). Without loss of generality, the subsequent development is based on the translation error for the feature point $i = 1$. The translation objective can be stated as

$$\| e(t) \| \to 0 \quad \text{as } t \to \infty \tag{24}$$

The subsequent section will target the control development based on the objectives in (22) and (24).

DOI: 10.1002/rnc

5. QUATERNION ESTIMATION

The control objective is defined as the desire to regulate the rotation matrix to the identity matrix (or equivalently to regulate the norm of the vector component of the quaternion to zero as in (22)). As the rotation matrix is not available due to uncertainty in the intrinsic camera calibration matrix, an estimated rotation matrix can be formulated from the development in (11)–(14). The development in this section focuses on developing a quaternion estimate that can related to the real quaternion (i.e. developing estimates $\hat{q}_0(t)$ and $\hat{q}_v(t)$ for $q_0(t)$ and $q_v(t)$), as a means to formulate a measurable error system that is meaningful.

To facilitate the development of a quaternion estimate, (20) and (21) are used to express the scalar component of the quaternion in terms of the rotation matrix $R(t)$ as [31]

$$q_0^2 = \frac{\text{tr}(R)+1}{4}$$

where $q_0(t)$ is restricted without loss of generality (this restriction enables the minimum rotation to be obtained) to be non-negative as

$$q_0 = \tfrac{1}{2}\sqrt{1+\text{tr}(R)} \tag{25}$$

where $\text{tr}(R)$ denotes the trace of $R(t)$. Based on the definition of a quaternion and the relationship in (25), $q_v(t)$ can be determined as

$$q_v = \pm u\sqrt{1-q_0^2} = \pm\tfrac{1}{2}u\sqrt{3-\text{tr}(R)} \tag{26}$$

where the rotation axis $u(t)$ is the unit eigenvector with respect to the eigenvalue 1 of $R(t)$. For the quaternion vector in (26), the sign ambiguity can be resolved. Specifically, (21) can be used to develop the following expression:

$$R^{\text{T}} - R = 4q_0 q_v^{\times} \tag{27}$$

As the sign of $q_0(t)$ is restricted (i.e. assumed to be) positive, then a unique solution for $q_v(t)$ can be determined from (26) and (27).

Based on the similarity between $\hat{R}(t)$ and $R(t)$ as stated in (14), the expressions in (25) and (26) provide motivation to develop the quaternion estimate as

$$\hat{q}_0 = \tfrac{1}{2}\sqrt{1+\text{tr}(\hat{R})} \tag{28}$$

$$\hat{q}_v = \pm\tfrac{1}{2}\hat{u}\sqrt{3-\text{tr}(\hat{R})} \tag{29}$$

In (28) and (29), $\hat{R}(t)$ is the estimated rotation matrix introduced in (13) that is computed from the homography decomposition. As $\hat{R}(t)$ is similar to $R(t)$ (see (14)), $\hat{R}(t)$ is guaranteed to have an eigenvalue of 1, where $\hat{u}(t)$ is the unit eigenvector that can be computed from the eigenvalue of 1. As $\hat{R}(t)$ is not guaranteed to be a true rotation matrix (and it will not be in general), the relationships in (21) and (27) cannot be developed and used to eliminate the sign ambiguity of the eigenvector $\hat{u}(t)$. However, the subsequent stability analysis and simulation results indicate that the same stability result is obtained invariant of the sign of $\hat{u}(t)$. Once the initial sign of $\hat{u}(t)$ is chosen, the same sign can be used for subsequent computations.

Based on the fact that $\hat{R}(t)$ is similar to $R(t)$ (see (14)), the properties that similar matrices have the same trace and eigenvalues can be used to relate the quaternion estimate and the actual quaternion. As similar matrices have the same trace, (25) and (28) can be used to conclude that

$$\hat{q}_0 = q_0 \tag{30}$$

As stated earlier, since similar matrices have the same eigenvalues, $\hat{R}(t)$ is guaranteed to have an eigenvalue of 1 with the associated eigenvector $\hat{u}(t)$. The following relationships can be developed based on (14):

$$\hat{u} = \hat{R}\hat{u} = \tilde{A}R\tilde{A}^{-1}\hat{u} \tag{31}$$

Premultiplying $\tilde{A}^{-1}$ on both sides of (31) yields

$$\tilde{A}^{-1}\hat{u} = R\tilde{A}^{-1}\hat{u} \tag{32}$$

Hence, $\tilde{A}^{-1}\hat{u}(t)$ is an eigenvector with respect to the eigenvalue 1 of $R(t)$ that can be expressed as

$$\tilde{A}^{-1}\hat{u} = \pm\gamma u \tag{33}$$

DOI: 10.1002/rnc

where $\gamma(t) \in \mathbb{R}$ is a positive scaling term defined as

$$\gamma = \frac{1}{\|\tilde{A}u\|} \tag{34}$$

Based on (26), (29), and (33), the estimated quaternion vector can now be related to the actual quaternion vector as

$$\hat{q}_v = \pm\gamma\tilde{A}q_v \tag{35}$$

As indicated in [32], the estimates $\hat{q}_0(t)$ and $\hat{q}_v(t)$ satisfy the nonlinear constraint for a unit quaternion given in (20). As also indicated in [32], the expression for $\gamma(t)$ given in (34) can also be written as

$$\gamma = \frac{\|q_v\|}{\|\tilde{A}q_v\|} \tag{36}$$

6. CONTROL DEVELOPMENT

The subsequent control design is focused on developing a kinematic (i.e. linear and angular velocity) controller for a camera with unconstrained motion. Owing to the structure of the developed controller, standard backstepping methods [33] can be applied to incorporate the robot dynamics. As discussed in detail in [34], the inclusion of the dynamic model of the camera positioning device will likely result in improved robustness and performance of the overall system. Some example results that include the dynamics of a robotic system include [3, 5, 7–9, 34–38].

6.1. Rotation control

The rotation open-loop error system can be developed by taking the time derivative of $q(t)$ as [39]

$$\begin{bmatrix} \dot{q}_0 \\ \dot{q}_v \end{bmatrix} = \frac{1}{2}\begin{bmatrix} -q_v^{\mathrm{T}} \\ q_0 I_3 + q_v^{\times} \end{bmatrix}\omega_{\mathrm{c}} \tag{37}$$

where $\omega_{\mathrm{c}}(t) \in \mathbb{R}^3$ denotes the angular velocity of the camera with respect to $\mathscr{F}^*$ expressed in $\mathscr{F}$. Based on the open-loop error system in (37) and the subsequent stability analysis, the angular velocity controller is designed as

$$\omega_{\mathrm{c}} = -K_\omega \hat{q}_v \tag{38}$$

where $K_\omega \in \mathbb{R}$ denotes a positive control gain. Substituting (38) into (37), the rotation closed-loop error system can be developed as

$$\dot{q}_0 = \tfrac{1}{2}K_\omega q_v^{\mathrm{T}}\hat{q}_v \tag{39}$$

$$\dot{q}_v = -\tfrac{1}{2}K_\omega(q_0 I_3 + q_v^{\times})\hat{q}_v \tag{40}$$

6.2. Translation control[¶]

As stated previously, translation controllers such as the class developed in [20, 21] can be combined with the developed quaternion-based rotation controller. To facilitate the subsequent stability analysis for the six DOF problem, a translation controller proposed in [20] is provided in this section. Specifically, one of the translation controllers in [20] is given by

$$v_c = (K_{v1} + K_{v2})\hat{e} \tag{41}$$

where $K_{v1}, K_{v2} \in \mathbb{R}$ denote positive constant control gains, and $\hat{e}(t) \in \mathbb{R}^3$ is defined as

$$\hat{e} = \frac{z_1}{z_1^*}\hat{m}_1 - \hat{m}_1^* \tag{42}$$

where $\hat{m}_1(t)$ and $\hat{m}_1^*$ can be computed from (8) and (9), respectively, and the ratio z_1/z_1^* can be computed from the decomposition of the estimated Euclidean homography in (11). The open-loop translation error system can be determined as [20]

$$\dot{e} = -\frac{1}{z_1^*}v_c - \omega_{\mathrm{c}}^{\times}e + [m_1^*]^{\times}\omega_{\mathrm{c}} \tag{43}$$

After substituting (38) and (41) into (43), the resulting closed-loop translation error system can be determined as

$$\dot{e} = \left(-(K_{v1} + K_{v2})\frac{1}{z_1^*}\tilde{A} + [K_\omega\hat{q}_v]^{\times}\right) \times e - K_\omega[m_1^*]^{\times}\hat{q}_v \tag{44}$$

[¶]The contribution of this paper is the rotation estimate and associated control development. The translation controller developed in this section is provided for completeness.

DOI: 10.1002/rnc

7. STABILITY ANALYSIS

As stated previously, the quaternion estimate $\hat{q}_v(t)$ has a sign ambiguity, but either choice of the sign will yield the same stability result. The following analysis is developed for the case where

$$\hat{q}_v = \gamma \tilde{A} q_v \tag{45}$$

A remark is provided at the end of the analysis, which describes how the stability can be proven for the case when

$$\hat{q}_v = -\gamma \tilde{A} q_v$$

Theorem 1
The controller given in (38) and (41) ensures asymptotic regulation in the sense that

$$\|q_v(t)\| \to 0, \quad \|e(t)\| \to 0 \quad \text{as } t \to \infty \tag{46}$$

provided that the following inequalities are satisfied [20, 21]:

$$\lambda_{\min}\{\tfrac{1}{2}(\tilde{A} + \tilde{A}^{\mathrm{T}})\} \geqslant \lambda_0 \tag{47}$$

$$\lambda_{\max}\{\tfrac{1}{2}(\tilde{A} + \tilde{A}^{\mathrm{T}})\} \leqslant \lambda_1 \tag{48}$$

where $\lambda_0, \lambda_1 \in \mathbb{R}$ are known positive constants, and the control gains K_{v1}, K_{v2}, and K_ω are selected based on the following sufficient conditions:

$$K_{v1} > \frac{z_1^* K_\omega \|m_1^*\|^2}{4\lambda_0^2 \sqrt{\dfrac{1}{\lambda_{\max}(\tilde{A}^{\mathrm{T}}\tilde{A})}}}$$
$$K_{v2} > \frac{z_1^* K_\omega}{\lambda_0} \sqrt{\frac{1}{\lambda_{\min}(\tilde{A}^{\mathrm{T}}\tilde{A})}} \tag{49}$$

where known upper bounds are assumed to exist for the unknown constants z_1^*, m_1^*.

Proof
Let $V(t) \in \mathbb{R}$ denote the following differentiable non-negative function (i.e. a Lyapunov candidate):

$$V = q_v^{\mathrm{T}} q_v + (1 - q_0)^2 + e^{\mathrm{T}} e \tag{50}$$

After cancelling common terms, $\dot{V}(t)$ can be expressed as

$$\dot{V} = -\gamma K_\omega q_v^{\mathrm{T}} \tilde{A} q_v - (K_{v1} + K_{v2}) \frac{1}{z_1^*} e^{\mathrm{T}} \tilde{A} e + \gamma e^{\mathrm{T}} \times [K_\omega \hat{q}_v]^\times e - \gamma K_\omega e^{\mathrm{T}} [m_1^*]^\times \tilde{A} q_v \tag{51}$$

Based on (36), (47) and the facts that

$$\|[\xi]^\times\|_2 = \|\xi\| \forall \xi \in \mathbb{R}^3 \quad \text{and} \quad \|\hat{q}_v\| \leqslant 1$$

the expression in (51) can be upper bounded as

$$\dot{V} \leqslant -\gamma K_\omega \lambda_0 \|q_v\|^2 - \frac{\lambda_0}{z_1^*}\left(K_{v2} - \frac{z_1^* \gamma K_\omega}{\lambda_0}\right)\|e\|^2 + K_\omega \|m_1^*\| \|q_v\| \|e\| - \frac{1}{z_1^*} K_{v1} \lambda_0 \|e\|^2 \tag{52}$$

After completing the squares on the last two terms, the inequality (52) can be rewritten as

$$\dot{V} \leqslant -\frac{K_\omega \lambda_0 \gamma}{K_{v1}}\left(K_{v1} - \frac{z_1^* K_\omega \|m_1^*\|^2}{4\lambda_0^2 \gamma}\right)\|q_v\|^2 - \frac{\lambda_0}{z_1^*}\left(K_{v2} - \frac{z_1^* \gamma K_\omega}{\lambda_0}\right)\|e\|^2 \tag{53}$$

Provided that the sufficient conditions given in (47)–(49) are satisfied,[‖] the inequality in (53) can be upper bounded as

$$\dot{V} \leqslant -c_1 \|q_v\|^2 - c_2 \|e\|^2 \tag{54}$$

where $c_1, c_2 \in \mathbb{R}$ are positive bounding constants. Based on (50) and (54), standard signal chasing arguments can be used to conclude that the control inputs and all the closed-loop signals are bounded. The expression in (54) can also be used to conclude that $q_v(t)$ and $e(t) \in \mathcal{L}_2$. As $q_v(t), \dot{q}_v(t), e(t), \dot{e}(t) \in \mathcal{L}_\infty$ and $q_v(t), e(t) \in \mathcal{L}_2$, Barbalat's Lemma [40] can be used to prove the result given in (46). □

[‖] See the Appendix for details regarding the development of the sufficient condition for the control gains K_{v1}, K_{v2}, and K_ω.

DOI: 10.1002/rnc

Remark 1
By modifying the Lyapunov function in (50) as follows:

$$V = q_v^{\mathrm{T}} q_v + (1+q_0)^2 + e^{\mathrm{T}} e$$

the same stability analysis arguments can be used to prove Theorem 1 for the case when

$$\hat{q}_v = -\gamma \tilde{A} q_v$$

8. SIMULATION RESULTS AND DISCUSSION

Numerical simulations were performed to illustrate the performance of the controller given in (38) and (41) for different camera calibration estimates. The actual intrinsic camera calibration matrix is given by

$$A = \begin{bmatrix} 122.5 & -3.77 & 100 \\ 0 & 122.56 & 100 \\ 0 & 0 & 1 \end{bmatrix}$$

The simulation was designed so that the camera would view an object with four coplanar feature points with the following Euclidean coordinates (in (m)):

$$\begin{aligned} O_1 &= [0.05 \;\; 0.05 \;\; 0]^{\mathrm{T}} \\ O_2 &= [0.05 \;\; -0.05 \;\; 0]^{\mathrm{T}} \\ O_3 &= [-0.05 \;\; 0.05 \;\; 0]^{\mathrm{T}} \\ O_4 &= [-0.05 \;\; -0.05 \;\; 0]^{\mathrm{T}} \end{aligned} \tag{55}$$

The normalized coordinates of the vanishing points were selected as

$$[0.02 \;\; 0.02 \;\; 1]^{\mathrm{T}} \quad [0.02 \;\; -0.02 \;\; 1]^{\mathrm{T}}$$

$$[-0.02 \;\; 0.02 \;\; 1]^{\mathrm{T}} \quad [-0.02 \;\; -0.02 \;\; 1]^{\mathrm{T}}$$

An orthogonal coordinate frame $\mathcal{I}$ was encoded with the z-axis opposite to n^* (see Figure 1) with the x-axis and y-axis on the plane π. The rotation matrices R_1 between $\mathcal{F}$ and $\mathcal{I}$, and R_2 between $\mathcal{F}^*$ and $\mathcal{I}$ were set as

$$R_1 = R_x(160^\circ) R_y(30^\circ) R_z(-30^\circ)$$

$$R_2 = R_x(120^\circ) R_y(-20^\circ) R_z(80^\circ)$$

where $R_x(\cdot)$, $R_y(\cdot)$, and $R_z(\cdot) \in SO(3)$ denote rotation of angle '$\cdot$' (degrees) along the x-axis, y-axis, and z-axis, respectively. The translation vectors $x_{f1}(t)$ and $x_{f2}(t)$ between $\mathcal{F}$ and $\mathcal{I}$ (expressed in $\mathcal{F}$) and between $\mathcal{F}^*$ and $\mathcal{I}$ (expressed in $\mathcal{F}^*$), respectively, were selected as

$$x_{f1} = [0.5 \;\; 0.5 \;\; 2.5]^{\mathrm{T}} \tag{56}$$

$$x_{f2} = [1.0 \;\; 1.0 \;\; 3.5]^{\mathrm{T}} \tag{57}$$

The initial (i.e. $p_i(0)$) and desired (i.e. p_i^*) image-space coordinates of the four feature points in (55) were computed as (in pixels)

$$\begin{aligned} p_1(0) &= [126.50 \;\; 123.64 \;\; 1]^{\mathrm{T}} \\ p_2(0) &= [124.24 \;\; 127.91 \;\; 1]^{\mathrm{T}} \\ p_3(0) &= [120.92 \;\; 125.40 \;\; 1]^{\mathrm{T}} \\ p_4(0) &= [123.25 \;\; 121.11 \;\; 1]^{\mathrm{T}} \\ p_1^* &= [132.17 \;\; 133.17 \;\; 1]^{\mathrm{T}} \\ p_2^* &= [135.72 \;\; 133.61 \;\; 1]^{\mathrm{T}} \\ p_3^* &= [135.71 \;\; 136.91 \;\; 1]^{\mathrm{T}} \\ p_4^* &= [132.10 \;\; 136.44 \;\; 1]^{\mathrm{T}} \end{aligned}$$

The initial (i.e. $p_{vi}(0)$) and desired (i.e. p_{vi}^*) image-space coordinates of the four vanishing points in (55) were computed as (in pixels)

$$\begin{aligned} p_{v1}(0) &= [124.02 \;\; 139.34 \;\; 1]^{\mathrm{T}} \\ p_{v2}(0) &= [129.02 \;\; 141.61 \;\; 1]^{\mathrm{T}} \\ p_{v3}(0) &= [131.02 \;\; 136.54 \;\; 1]^{\mathrm{T}} \\ p_{v4}(0) &= [126.03 \;\; 134.35 \;\; 1]^{\mathrm{T}} \\ p_{v1}^* &= [102.37 \;\; 102.45 \;\; 1]^{\mathrm{T}} \\ p_{v2}^* &= [102.53 \;\; 97.55 \;\; 1]^{\mathrm{T}} \\ p_{v3}^* &= [97.63 \;\; 97.55 \;\; 1]^{\mathrm{T}} \\ p_{v4}^* &= [97.47 \;\; 102.45 \;\; 1]^{\mathrm{T}} \end{aligned}$$

DOI: 10.1002/rnc

To test the performance of the controller under different camera calibration estimates, three simulations were performed. For the first simulation, the best-guess estimate for A was selected based on a conservative estimate of the results that would be obtained from a typical calibration. Typical camera calibration routines can provide calibration estimates within 3% of error. In addition, typical cameras have little to no skew, and the image center is exactly known for digital cameras. For the first simulation, the calibration estimate

$$\hat{A}=\begin{bmatrix}100 & -4 & 80\\ 0 & 100 & 110\\ 0 & 0 & 1\end{bmatrix}$$

contained approximately 20% of error for the parameters. The resulting calibration mismatch matrix is given as

$$\tilde{A}=\begin{bmatrix}1.225 & 0.0113 & 0.196\\ 0 & 1.226 & -0.1\\ 0 & 0 & 1\end{bmatrix}$$

where the minimum and maximum eigenvalues of $\frac{1}{2}(\tilde{A}+\tilde{A}^{\mathrm{T}})$ fall between 0.95 and 1.27, which meet the conditions given in (47) and (48). The control gains K_ω in (38) and K_{v1} and K_{v2} in (41) were selected as

$$K_\omega=5,\quad K_{v1}=2,\quad K_{v2}=3 \tag{58}$$

Given the selection of $K_\omega=5$ and estimates for the upper bounds of $z_1^*=3$ and $\|m_1^*\|=1$ (the actual values of z_1^* and $\|m_1^*\|$ are 2.53 and 0.75, respectively), the control gains K_{v1} and K_{v2} should be selected as

$$K_{v1}=5.23,\quad K_{v2}=16.37$$

based on the sufficient gain conditions given in (49). As is typical with Lyapunov analysis, the developed sufficient gain conditions are very conservative. The simulation results for this simulation (and the following two simulations) use gain values that are well below the indicated sufficient conditions. The resulting translation and rotation errors are plotted in Figures 2 and 3, respectively. The image-space pixel error (i.e. $p_i(t)-p_i^*$) is shown in Figure 4, and is also depicted in Figure 5 in a 3D format. The translation and rotation

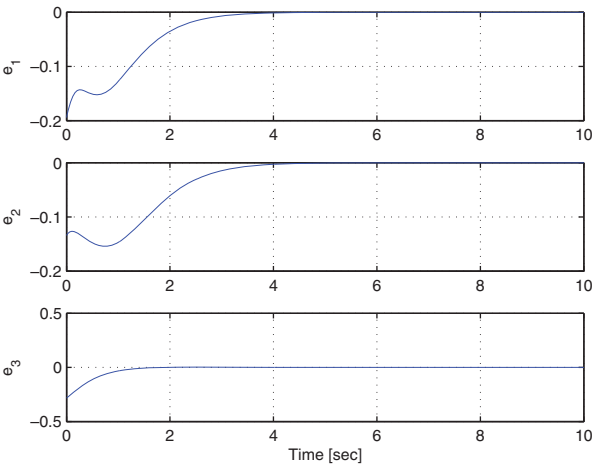

Figure 2. Unitless translation error between $m_1(t)$ and m_1^*.

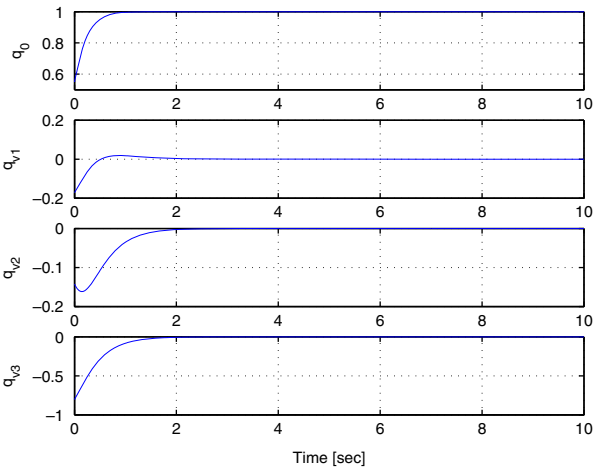

Figure 3. Quaternion rotation error.

control outputs are shown in Figures 6 and 7, respectively. Different results can be obtained with different gain selections.

Order of magnitude calibration errors are well beyond typical inaccuracies. Yet, to illustrate the robustness of the developed controller and the mildness of the developed sufficient condition on the static calibration estimate, the second and third simulations are based on calibration errors that are an order of magnitude too large or too small, respectively. For the second simulation, the estimate for the product of the scale factor and focal length was selected to be an

DOI: 10.1002/rnc

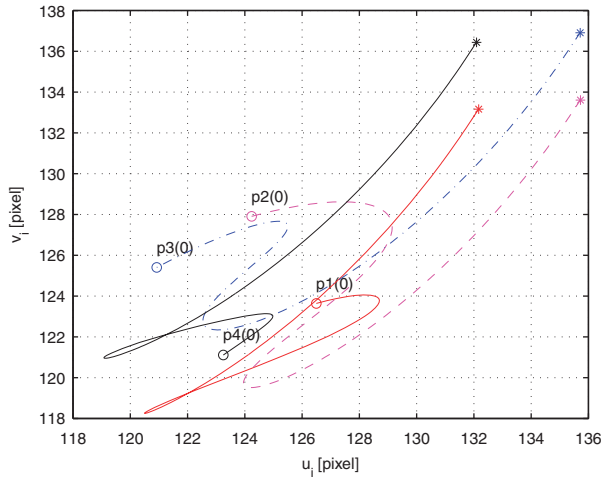

Figure 4. Image-space error in pixles between $p_i(t)$ and p_i^*. In the figure, 'O' denotes the initial positions of the four feature points in the image, and '*' denotes the corresponding final positions of the feature points.

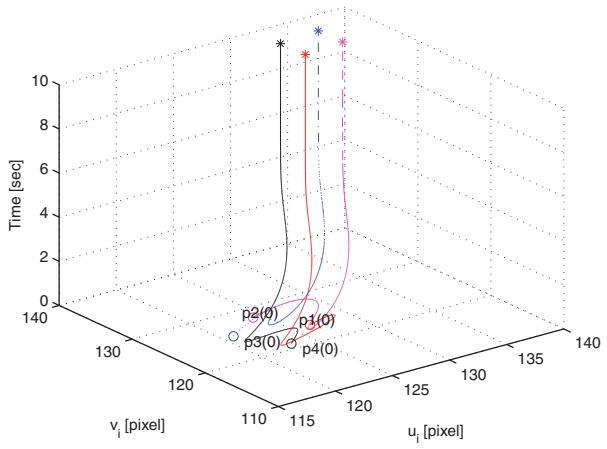

Figure 5. Image-space error in pixles between $p_i(t)$ and p_i^* shown in a 3D graph. In the figure, 'O' denotes the initial positions of the four feature points in the image, and '*' denotes the corresponding final positions of the feature points.

order of magnitude greater than the actual values as

$$\hat{A} = \begin{bmatrix} 1225 & -4 & 80 \\ 0 & 1225.6 & 110 \\ 0 & 0 & 1 \end{bmatrix}$$

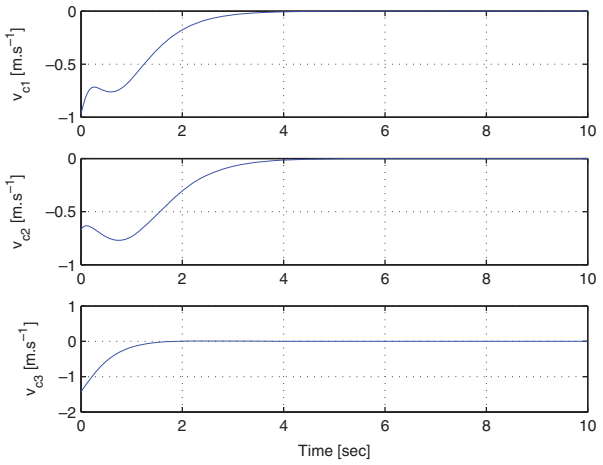

Figure 6. Linear camera velocity control input.

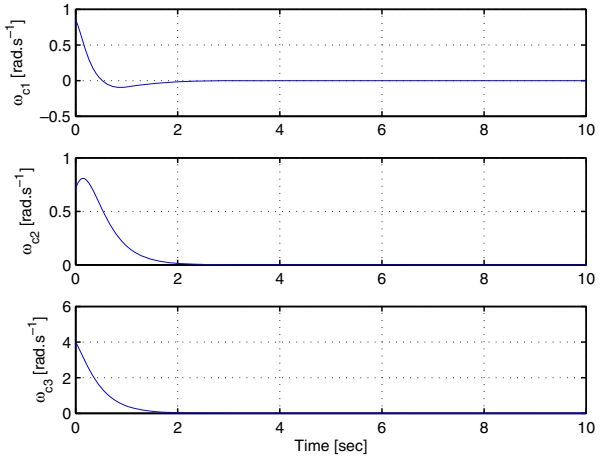

Figure 7. Angular camera velocity control input.

resulting in the estimation error matrix

$$\tilde{A} = \begin{bmatrix} 0.1 & -0.003 & 0.016 \\ 0 & 0.1 & -0.008 \\ 0 & 0 & 1 \end{bmatrix}$$

where the minimum and maximum eigenvalues of $\frac{1}{2}(\tilde{A}+\tilde{A}^{\mathrm{T}})$ fall between 0.1 and 1.0. The control gains

DOI: 10.1002/rnc

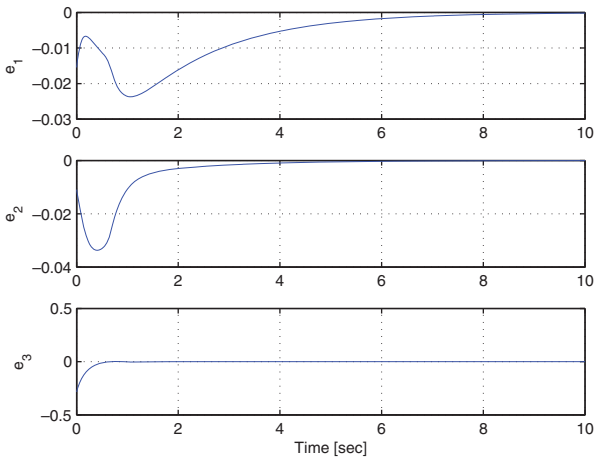

Figure 8. Unitless translation error between $m_1(t)$ and m_1^*.

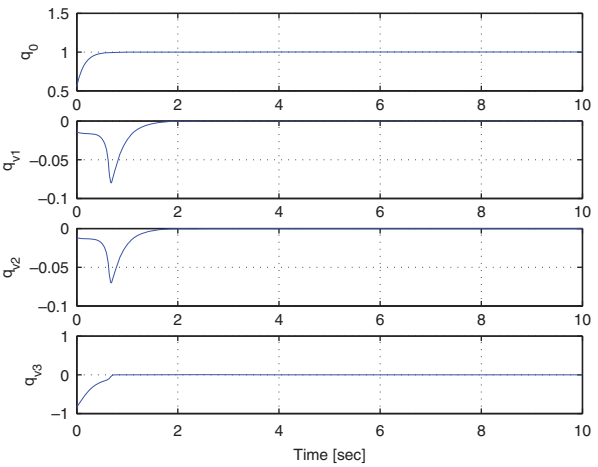

Figure 9. Quaternion rotation error.

K_ω in (38) and K_{v1} and K_{v2} in (41) were selected as

$$K_\omega = 8, \quad K_{v1} = 5, \quad K_{v2} = 15$$

where the sufficient gain condition (under the same estimates for z_1^* and $\|m_1^*\|$) for K_{v1} and K_{v2} computed using (49) are

$$K_{v1} = 385, \quad K_{v2} = 1542$$

The resulting translation and rotation errors are given in Figures 8 and 9, respectively.

For the third simulation, the estimate for the product of the scale factor and focal length was selected to be an order of magnitude less than the actual values as follows:

$$\hat{A} = \begin{bmatrix} 12.25 & -4 & 80 \\ 0 & 12.256 & 110 \\ 0 & 0 & 1 \end{bmatrix}$$

resulting in the estimation error matrix

$$\tilde{A} = \begin{bmatrix} 10.0 & 2.96 & 1.37 \\ 0 & 10.0 & -0.82 \\ 0 & 0 & 1 \end{bmatrix}$$

where the minimum and maximum eigenvalues of $\frac{1}{2}(\tilde{A} + \tilde{A}^{\mathrm{T}})$ fall between 0.92 and 11.48. The control gains K_ω in (38) and K_{v1} and K_{v2} in (41) were selected as

$$K_\omega = 3, \quad K_{v1} = 1, \quad K_{v2} = 2$$

where the sufficient gain condition (under the same estimates for z_1^* and $\|m_1^*\|$) for K_{v1} and K_{v2} computed using (49) are

$$K_{v1} = 51.60, \quad K_{v2} = 16.60$$

The resulting translation and rotation errors are plotted in Figures 10 and 11, respectively.

9. CONCLUSIONS

The seminal work by Malis and Chaumette [19] provided a new method to develop visual servo controllers for the six DOF problem. Since then, a plethora of 2.5D or homography-based visual servo control results have been developed. A common characteristic with all of these results is that they rely on the axis–angle rotation parameterization to develop the rotation error system, and most results require the camera calibration matrix to be known. Some recent homography-based methods have been proven to yield asymptotic convergence despite uncertainty in the camera calibration. However, the methods rely heavily

DOI: 10.1002/rnc

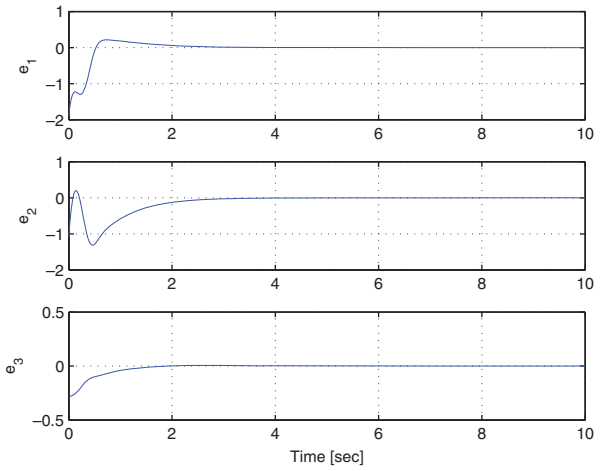

Figure 10. Unitless translation error between $m_1(t)$ and m_1^*.

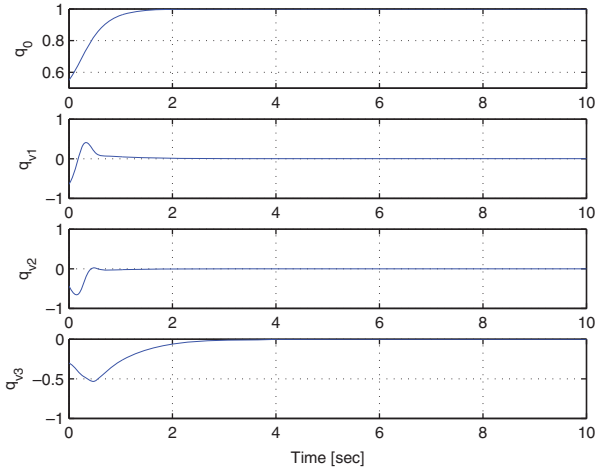

Figure 11. Quaternion rotation error.

on properties that originate from the axis–angle parameterization. Some applications are better suited for a non-singular parameterization such as the quaternion. The research in this paper sought to answer the question: *Can state estimates and a measurable closed-loop error system be crafted in terms of the quaternion parameterization when the camera calibration parameters are unknown*? To provide an affirmative answer to the question, a similarity relationship between an estimated and the actual rotation matrices was used to both construct a quaternion-based rotation estimate and to relate the estimated quaternion to the actual quaternion. This relationship was then used to construct a measurable controller and a closed-loop rotation error system for the actual quaternion error. A translation error system from literature was then combined with the new quaternion rotation error system in a Lyapunov-based stability analysis. Although the sign of the quaternion estimate cannot be determined, a unique controller was developed that achieves asymptotic regulation invariant of the sign ambiguity. A potential limitation of the developed method (and other homography-based methods that have been developed for uncertain camera calibration) is the use of a sufficient condition that the calibration estimate is selected sufficiently close to the actual values. Simulation results are provided to validate the proposed visual servo approach, even in the presence of an order of magnitude errors in the calibration estimate.

APPENDIX A: CONTROL GAIN SUFFICIENT CONDITION DEVELOPMENT

From the expression in (53), $\dot{V}(t)$ is negative semi-definite if the following inequalities are satisfied:

$$K_{v1} > \frac{z_1^* K_\omega \|m_1^*\|^2}{4\lambda_0^2 \gamma}, \quad K_{v2} > \frac{z_1^* \gamma K_\omega}{\lambda_0} \tag{A1}$$

Based on the definition of the positive scaling term in (34), $\gamma^2(t)$ can be expressed as

$$\gamma^2 = \frac{u^{\mathrm{T}} u}{u^{\mathrm{T}} \tilde{A}^{\mathrm{T}} \tilde{A} u}$$

As $\tilde{A}$ is full rank, the symmetric matrix $\tilde{A}^{\mathrm{T}}\tilde{A}$ is positive definite, and the Rayleigh–Ritz theorem can be used to conclude that

$$\lambda_{\min}(\tilde{A}^{\mathrm{T}}\tilde{A})\|u\|^2 \leqslant u^{\mathrm{T}}\tilde{A}^{\mathrm{T}}\tilde{A}u \leqslant \lambda_{\max}(\tilde{A}^{\mathrm{T}}\tilde{A})\|u\|^2$$

where $\lambda_{\min}(\tilde{A}^{\mathrm{T}}\tilde{A})$ and $\lambda_{\max}(\tilde{A}^{\mathrm{T}}\tilde{A})$ denote the minimal and maximum eigenvalues of $\tilde{A}^{\mathrm{T}}\tilde{A}$, respectively. Using

DOI: 10.1002/rnc

the facts that $\gamma(t) > 0$ and $\|u(t)\|^2 = 1$, the following inequalities can be developed:

$$\sqrt{\frac{1}{\lambda_{\max}(\tilde{A}^{\mathrm{T}}\tilde{A})}} \leqslant \gamma \leqslant \sqrt{\frac{1}{\lambda_{\min}(\tilde{A}^{\mathrm{T}}\tilde{A})}} \tag{A2}$$

Based on the inequalities in (A2), the sufficient conditions in (A1) can be expressed as in (49).

ACKNOWLEDGEMENTS

This research is supported in part by the NSF CAREER award CMS-0547448, AFOSR contract numbers F49620-03-1-0381 and F49620-03-1-0170, AFRL contract number FA4819-05-D-0011, and by research grant No. US-3715-05 from BARD, the United States–Israel Binational Agricultural Research and Development Fund at the University of Florida, and in part by the startup fund at the Kansas State University.

REFERENCES

1. Astolfi A, Hsu L, Netto M, Ortega R. Two solutions to the adaptive visual servoing problem. *IEEE Transactions on Robotics and Automation* 2002; **18**(3):387–392.
2. Bishop B, Hutchinson S, Spong M. Camera modeling for visual servo control applications. *Mathematical and Computer Modeling* 1996; **24**(5/6):79–102.
3. Dixon WE, Dawson DM, Zergeroglu E, Behal A. Adaptive tracking control of a wheeled mobile robot via an uncalibrated camera system. *IEEE Transactions on Systems, Man, and Cybernetics—Part B: Cybernetics* 2001; **31**(3):341–352.
4. Hsu L, Aquino PLS. Adaptive visual tracking with uncertain manipulator dynamics and uncalibrated camera. *Proceedings of the IEEE Conference on Decision and Control*, Phoenix, AZ, U.S.A., 1999; 1248–1253.
5. Kelly R. Robust asymptotically stable visual servoing of planar robots. *IEEE Transactions on Robotics and Automation* 1996; **12**(5):759–766.
6. Kelly R, Marquez A. Fixed-eye direct visual feedback control of planar robots. *Journal of Systems Engineering* 1995; **4**(5):239–248.
7. Zergeroglu E, Dawson DM, de Queiroz M, Behal A. Vision-based nonlinear tracking controllers in the presence of parametric uncertainty. *IEEE/ASME Transactions on Mechatronics* 2001; **6**(3):322–337.
8. Zergeroglu E, Dawson DM, de Queiroz M, Nagarkatti S. Robust visual-servo control of planar robot manipulators in the presence of uncertainty. *Proceedings of the IEEE Conference on Decision and Control*, Phoenix, AZ, U.S.A., 1999; 4137–4142.
9. Liu Y, Wang H, Wang C, Lam K. Uncalibrated visual servoing of robots using a depth-independent interaction matrix. *IEEE Transactions on Robotics* 2006; **22**(4):804–817.
10. Liu Y, Wang H, Lam K. Dynamic visual servoing of robots in uncalibrated environments. *Proceedings of the IEEE International Conference on Robotics and Automation*, Barcelona, Spain, 2005; 3142–3148.
11. Liu Y, Wang H, Zhou D. Dynamic tracking of manipulators using visual feedback from an uncalibrated fixed camera. *Proceedings of the IEEE International Conference on Robotics and Automation*, Orlando, FL, U.S.A., 2006; 4124–4129.
12. Piepmeier JA, McMurray GV, Lipkin H. A dynamic jacobian estimation method for uncalibrated visual servoing. *Proceedings of the IEEE/ASME International Conference on Advanced Intelligent Mechatronics*, Atlanta, GA, U.S.A., 1999; 944–949.
13. Piepmeier JA, McMurray GV, Lipkin H. Uncalibrated dynamic visual servoing. *IEEE Transactions on Robotics and Automation* 2004; **20**(1):143–147.
14. Piepmeier JA, McMurray GV, Lipkin H. A dynamic quasi-Newton method for uncalibrated visual servoing. *Proceedings of the IEEE International Conference on Robotics and Automation*, Detroit, MI, U.S.A., 1999; 1595–1600.
15. Piepmeier JA, Gumpert BA, Lipkin H. Uncalibrated eye-in-hand visual servoing. *Proceedings of the IEEE International Conference on Robotics and Automation*, Washington, DC, U.S.A., 2002; 568–573.
16. Piepmeier JA. Experimental results for uncalibrated eye-in-hand visual servoing. *Southeastern Symposium on System Theory*, Morgantown, WV, U.S.A., 2003; 335–339.
17. Shahamiri M, Jagersand M. Uncalibrated visual servoing using a biased Newton method for on-line singularity detection and avoidance. *Proceedings of the IEEE/RSJ International Conference on Intelligent Robots and Systems*, Edmonton, Alberta, Canada, 2005; 3953–3958.
18. Malis E. Visual servoing invariant to changes in camera-intrinsic parameters. *IEEE Transactions on Robotics and Automation* 2004; **20**(1):72–81.
19. Malis E, Chaumette F, Boudet S. 2–1/2-D visual servoing. *IEEE Transactions on Robotics and Automation* 1999; **15**(2): 238–250.
20. Fang Y, Dixon WE, Dawson DM, Chen J. An exponential class of model-free visual servoing controllers in the presence of uncertain camera calibration. *International Journal of Robotics and Automation* 2006; **21**(4):247–255.
21. Malis E, Chaumette F. Theoretical improvements in the stability analysis of a new class of model-free visual servoing methods. *IEEE Transactions on Robotics and Automation* 2002; **18**(2):176–186.
22. Hu G, Dixon WE, Gupta S, Fitz-coy N. A quaternion formulation for homography-based visual servo control. *Proceedings of the IEEE International Conference on Robotics and Automation*, Orlando, FL, U.S.A., 2006; 2391–2396.
23. Malis E, Chaumette F. 2 1/2 D visual servoing with respect to unknown objects through a new estimation scheme of camera

displacement. *International Journal of Computer Vision* 2000; **37**(1):79–97.
24. Faugeras O. *Three-Dimensional Computer Vision*: *A Geometric Viewpoint*. MIT Press: Cambridge, MA, 1993.
25. Shi J, Tomasi C. Good features to track. *Proceedings of the IEEE Conference on Computer Vision and Pattern Recognition*, Seattle, WA, U.S.A., 1994; 593–600.
26. Tomasi C, Kanade T. Detection and tracking of point features. *Technical Report*, Carnegie Mellon University, 1991.
27. Hartley R, Zisserman A. *Multiple View Geometry in Computer Vision*. Cambridge University Press: New York, 2000.
28. Fang Y, Behal A, Dixon WE, Dawson DM. Adaptive 2.5d visual servoing of kinematically redundant robot manipulators. *Proceedings of the IEEE Conference on Decision and Control*, Las Vegas, NV, U.S.A., 2002; 2860–2865.
29. Faugeras O, Lustman F. Motion and structure from motion in a piecewise planar environment. *International Journal of Pattern Recognition and Artificial Intelligence* 1988; **2**(3):485–508.
30. Zhang Z, Hanson AR. Scaled Euclidean 3d reconstruction based on externally uncalibrated cameras. *IEEE Symposium on Computer Vision*, Coral Gables, FL, U.S.A., 1995; 37–42.
31. Shuster M. A survey of attitude representations. *The Journal of the Astronautical Sciences* 1993; **41**(4):439–518.
32. Hu G. Visual servo tracking control via a Lyapunov-based approach. *Dissertation*, University of Florida, 2007.
33. Krstic M, Kanellakopoulos I, Kokotovic P. *Nonlinear and Adaptive Control Design*. Wiley: New York, 1995.
34. Corke P, Good M. Dynamic effects in visual closed-loop systems. *IEEE Transactions on Robotics and Automation* 1996; **12**(5):671–683.
35. Conticelli F, Allotta B. Two-level visual control of dynamic look-and-move systems. *Proceedings of the IEEE International Conference on Robotics and Automation*, San Francisco, CA, U.S.A., 2000; 3784–3789.
36. Behala, Setlur P, Dixon WE, Dawson DM. Adaptive position and orientation regulation for the camera-in-hand problem. *Journal of Robotic Systems* 2005; **22**(9):457–473.
37. Kelly R, Reyes F, Moreno J, Hutchinson S. A two-loops direct visual control of direct-drive planar robots with moving target. *Proceedings of the IEEE International Conference on Robotics and Automation* 1999; 599–604.
38. Kelly R, Carelli R, Nasisi O, Kuchen B, Reyes F. Stable visual servoing camera-in-hand robotic systems. *IEEE/ASME Transactions on Mechatronics* 2000; **5**(1): 39–48.
39. Dixon WE, Behal A, Dawson DM, Nagarkatti S. *Nonlinear Control of Engineering Systems*: *A Lyapunov-based Approach*. Birkhäuser: Boston, 2003.
40. Slotine JJ, Li W. *Applied Nonlinear Control*. Prentice-Hall, Inc.: Englewood Cliffs, NJ, 1991.

DOI: 10.1002/rnc